

Superstatistics as the thermodynamic limit of driven classical systems

Sergio Davis^{a,b}, Claudia Loyola^b, Carlos Femenías^b, Joaquín Peralta^b

^a*Research Center on the Intersection in Plasma Physics, Matter and Complexity, P²mc,
Comisión Chilena de Energía Nuclear, Casilla 188-D, Santiago, Chile*

^b*Departamento de Física, Facultad de Ciencias Exactas, Universidad Andres Bello,
Sazié 2212, piso 7, 8370136, Santiago, Chile.*

Abstract

Superstatistics is an elegant framework for the description of steady-state thermodynamics, mostly used for systems with long-range interactions such as plasmas. In this work, we show that the potential energy distribution of a classical system under externally imposed energy fluctuations can also be described by superstatistics in the thermodynamic limit. As an example, we apply this formalism to the thermodynamics of a finite Lennard-Jones crystal with constant microcanonical heat capacity driven by sinusoidal energy oscillations. Our results show that molecular dynamics simulations of the Lennard-Jones crystal are in agreement with the provided theoretical predictions.

1. Introduction

The thermodynamics of finite systems has gained attention recently, mostly in chemical physics [1, 2] and condensed matter physics [3] in connection with the non-equilibrium generalization of Boltzmann-Gibbs statistics known as superstatistics [4, 5]. This is motivated by the well-known failures in the thermodynamical description of small systems that exhibit significant deviations from the canonical behavior, especially near and below the critical point [3, 6]. In the superstatistics theory, commonly employed to describe systems with long-range interactions such as plasmas, self-gravitating systems and other complex systems, equilibrium is represented by a constant temperature, while non-equilibrium steady states are characterized by a statistical distribution of temperatures.

The superstatistical framework is clear and concise, expressing the idea of temperature fluctuations in a manner fully compatible with probability theory [7]. However, it has been shown [8, 9] that the description of the components of an isolated system needs to fulfill strict requirements to be compatible with superstatistics. For instance, if we divide an isolated system into two regions, superstatistics cannot describe one region if the other region has positive microcanonical heat capacity.

In this work, we illustrate the application of the superstatistical framework to describe a finite-size system having sinusoidal energy oscillations, a simple realization of a driven system. We show that superstatistics is in fact an accurate description when the superstatistical inverse temperature $\beta := 1/(k_B T)$ is taken to be the microcanonical inverse temperature. The rest of the paper is organized as follows. Section 2 presents a detailed review of the microcanonical distribution and the potential energy of the system. Sections 3 and 4 present a detailed review of the superstatistical framework and the thermodynamic limit for the case of sinusoidal energy oscillations; additionally, the theoretical results for the total and potential energy distributions are presented. Section 5 presents the molecular dynamics simulations for a Lennard-Jones (LJ) finite-size system used to test our theoretical results. Finally, we give some concluding remarks and discuss the scope of our work in Section 6.

Email address: sergio.davis@cchen.cl (Sergio Davis)

2. Microcanonical distribution of potential energy

In order to describe the probability density of potential energy of a classical finite-size system, we first begin with the particular case of fixed total energy, i.e. a microcanonical system. We will consider a system of N particles with Hamiltonian

$$\mathcal{H}(\mathbf{\Gamma}) = K(\mathbf{p}_1, \dots, \mathbf{p}_N) + \Phi(\mathbf{r}_1, \dots, \mathbf{r}_N), \quad (1)$$

where $\mathbf{\Gamma} = (\mathbf{r}_1, \dots, \mathbf{r}_N, \mathbf{p}_1, \dots, \mathbf{p}_N)$ is a point in phase space,

$$K(\mathbf{p}_1, \dots, \mathbf{p}_N) = \sum_{i=1}^N \frac{\mathbf{p}_i^2}{2m_i} \quad (2)$$

is the kinetic energy and $\Phi(\mathbf{R})$ the potential energy. If our system is isolated, then the energy is fixed at a value E and we have

$$P(\mathbf{r}_1, \dots, \mathbf{r}_N|E) = \frac{1}{\Omega(E)} \int d\mathbf{p}_1 \dots d\mathbf{p}_N \delta(E - K(\mathbf{p}_1, \dots, \mathbf{p}_N) - \Phi(\mathbf{r}_1, \dots, \mathbf{r}_N)) = \frac{\Omega_K(E - \Phi(\mathbf{r}_1, \dots, \mathbf{r}_N))}{\Omega(E)} \quad (3)$$

where Ω_K is the kinetic density of states, given by

$$\Omega_K(K) := \int d\mathbf{p}_1 \dots d\mathbf{p}_N \delta\left(\sum_{i=1}^N \frac{\mathbf{p}_i^2}{2m_i} - K\right) = W [K]_+^{\frac{3N}{2}-1}, \quad (4)$$

with W a constant and where the notation $[x]_+ = \max(0, x)$ is used. The microcanonical heat capacity is defined by

$$C_E := \left(\frac{dE}{dT}\right)_E = -k_B \frac{\beta_\Omega(E)^2}{\beta_\Omega'(E)} \quad (5)$$

where

$$\beta_\Omega(E) := \frac{1}{k_B T(E)} = \frac{\partial}{\partial E} \ln \Omega(E), \quad (6)$$

is the microcanonical inverse temperature. In this work we will be considering a system where C_E is a constant, let us say

$$C_E = \alpha k_B, \quad (7)$$

where α is an extensive, dimensionless constant. In this case we must have $E = \alpha k_B T(E)$, therefore

$$\beta_\Omega(E) = \frac{\alpha}{E} \quad (8)$$

and, by integration of (6), it follows that the full density of states $\Omega(E)$ must be of the form

$$\Omega(E) = \Omega_0 E^\alpha. \quad (9)$$

Using this we can write

$$P(\phi|E) = \int d\mathbf{R} \delta(\Phi(\mathbf{R}) - \phi) P(\mathbf{R}|E) = \frac{W}{\Omega(E)} [E - \phi]_+^{\frac{3N}{2}-1} \mathcal{D}(\phi), \quad (10)$$

where $\mathcal{D}(\phi)$ is the configurational density of states, defined by

$$\mathcal{D}(\phi) := \int d\mathbf{R} \delta(\Phi(\mathbf{R}) - \phi). \quad (11)$$

The distribution in (10) is the microcanonical distribution of potential energies introduced in the context of molecular simulation [10–12]. As we prove in [Appendix A](#), the only configurational density of states compatible with $\Omega(E)$ as in (9) has the form

$$\mathcal{D}(\phi) = D_0 \phi^{\alpha - \frac{3N}{2}}. \quad (12)$$

It is important to note that the exponent $\alpha - \frac{3N}{2}$ in (12) is exact for all $N \geq 1$. Replacing (12) we can impose normalization of the distribution to obtain

$$P(\phi|E) = \frac{\phi^{\alpha - \frac{3N}{2}} [E - \phi]_+^{\frac{3N}{2} - 1}}{B(\frac{3N}{2}, \alpha + 1 - \frac{3N}{2}) E^\alpha}, \quad (13)$$

where $B(a, b)$ is the beta function. The most probable value of ϕ given E , denoted by $\phi^*(E)$, can be determined from the extremum condition

$$0 = \left[\frac{\partial}{\partial \phi} \ln P(\phi|E) \right]_{\phi=\phi^*(E)} = -\frac{3N-2}{2(E-\phi^*(E))} + \frac{2\alpha-3N}{2\phi^*(E)} \quad (14)$$

from which it follows that

$$\phi^*(E) = \left[1 - \frac{3N-2}{2(\alpha-1)} \right] E. \quad (15)$$

In order to determine the moments of ϕ at constant E we will make use of the conjugate variables theorem [13, 14]. This identity is a consequence of the divergence theorem and relates expectations of derivatives with expectations involving logarithmic derivatives of the probability density. For a probability density $P(X|S)$ it has the form

$$\left\langle \frac{\partial \omega}{\partial X} \right\rangle_S + \left\langle \omega \frac{\partial}{\partial X} \ln P(X|S) \right\rangle_S = 0, \quad (16)$$

where $\omega(X)$ is an arbitrary, differentiable function of the variable X . In our case we have

$$\left\langle \frac{\partial \omega}{\partial \phi} \right\rangle_E = \left\langle \omega \left[\frac{3N-2}{2(E-\phi)} - \frac{2\alpha-3N}{2\phi} \right] \right\rangle_E \quad (17)$$

with $\omega(\phi)$ an arbitrary, differentiable function of ϕ . Using $\omega(\phi) = \phi^m (E - \phi)$ and after some algebra, we have the recurrence relation

$$(\alpha + m) \langle \phi^m \rangle_E = \left(\alpha + m - \frac{3N}{2} \right) E \langle \phi^{m-1} \rangle_E \quad (18)$$

which has solution

$$\langle \phi^m \rangle_E = E^m \prod_{k=1}^m \left(\frac{\alpha + k - \frac{3N}{2}}{\alpha + k} \right) = \frac{\Gamma(\alpha + 1) \Gamma(\alpha + m + 1 - \frac{3N}{2})}{\Gamma(\alpha + m + 1) \Gamma(\alpha + 1 - \frac{3N}{2})} E^m. \quad (19)$$

From here, using $m = 1$ we obtain the mean potential energy as

$$\langle \phi \rangle_E = \left[1 - \frac{3N}{2(\alpha + 1)} \right] E, \quad (20)$$

and, as expected, $\langle \phi \rangle_E \approx \phi^*(E)$ for $N \gg 1$ and $\alpha \gg 1$. Similarly, using $m = 2$ we obtain the relative variance

$$\frac{\langle (\delta\phi)^2 \rangle_E}{\langle \phi \rangle_E^2} = \frac{3N}{2(\alpha + 2)(\alpha - 3N/2 + 1)}. \quad (21)$$

The formula in (21) provides a finite-size version of the celebrated Lebowitz-Percus-Verlet [15] formula, used to calculate the heat capacity in atomistic computer simulations. Clearly, in the thermodynamic limit, $N \rightarrow \infty$ and $\alpha \rightarrow \infty$ so the relative variance of ϕ vanishes as $1/N$, as expected from equilibrium thermodynamics. It is also important to note, for the following sections, that

$$\left\langle \frac{3N-2}{2(E-\phi)} \right\rangle_E = \beta_\Omega(E) \quad (22)$$

for all sizes N , as can be deduced from the identity

$$0 = \left\langle \frac{\partial}{\partial E} \ln P(\phi|E) \right\rangle_E = \left\langle \frac{3N-2}{2(E-\phi)} - \frac{\alpha}{E} \right\rangle_E = \left\langle \frac{3N-2}{2(E-\phi)} \right\rangle_E - \beta_\Omega(E), \quad (23)$$

where we have replaced $P(\phi|E)$ as given in (13).

3. The superstatistical approximation in the thermodynamic limit

In this section we will generalize the microcanonical description of the previous section towards a steady state where energy does fluctuate, and formulate such a description in connection with the framework of superstatistics. Superstatistics [4, 5] is regarded as an elegant proposal among those that aim to describe non-equilibrium systems in steady states. It promotes the constant inverse temperature $\beta = 1/(k_B T)$ of the canonical ensemble to a random variable, having a joint distribution

$$P(\Gamma, \beta|S) = P(\Gamma|\beta)P(\beta|S) = \left[\frac{\exp(-\beta\mathcal{H}(\Gamma))}{Z(\beta)} \right] P(\beta|S), \quad (24)$$

with the microstates Γ . The marginal distribution of microstates is then given by

$$P(\Gamma|S) = \int_0^\infty d\beta P(\Gamma|\beta)P(\beta|S), \quad (25)$$

where we have integrated out the variable β . Replacing (24) we have that $P(\Gamma|S)$ is a superposition of canonical models that considers every possible value of β weighted by its probability density. That is, we can write

$$P(\Gamma|S) = \int_0^\infty d\beta P(\beta|S) \left[\frac{\exp(-\beta\mathcal{H}(\Gamma))}{Z(\beta)} \right]. \quad (26)$$

Therefore, our goal is to write a general ensemble $P(\Gamma|S)$ with an arbitrary distribution of energy $P(E|S)$ as an instance of (26) under a suitable definition of fluctuating temperature β and its distribution $P(\beta|S)$. The ensemble function for ϕ given E is

$$\rho(\phi; E) = \frac{W}{\Omega(E)} [E - \phi]_+^{\frac{3N}{2}-1} \quad (27)$$

such that $P(\phi|E) = \rho(\phi; E)\mathcal{D}(\phi)$ agrees with (10). If we lift the constraint of constant total energy, using the marginalization rule we can write

$$P(\phi|S) = \int_0^\infty dE P(E|S) \rho(\phi; E), \quad (28)$$

which implies

$$\rho(\phi; S) = \int_0^\infty dE P(E|S) \rho(\phi; E). \quad (29)$$

In the following, we will show that $\rho(\phi; S)$ in (29) reduces for $N \gg 1$ to a superstatistical ensemble function. First, we note that the factor

$$\mathcal{M}(\phi; E) := [E - \phi]_+^{\frac{3N}{2}-1} \quad (30)$$

can be rewritten as

$$\mathcal{M}(\phi; E) = (E - \phi_E)^{\frac{3N}{2}-1} \left[1 - \frac{\phi - \phi_E}{E - \phi_E} \right]_+^{\frac{3N}{2}-1} = (E - \phi_E)^{\frac{3N}{2}-1} \left[1 - (1-q)\beta_E \phi \right]_+^{\frac{1}{1-q}} \quad (31)$$

where we have introduced a reference potential energy ϕ_E , to be determined later, together with the quantities

$$q := 1 - \frac{2}{3N-2}, \quad (32a)$$

$$\beta_E := \frac{3N-2}{2(E - \phi_E)}. \quad (32b)$$

We can approximate the factor \mathcal{M} in (31) for $N \gg 1$ as

$$\mathcal{M}(\phi; E) \approx (E - \phi_E)^{\frac{3N}{2}} \exp(-\beta_E \phi), \quad (33)$$

so that normalization of (10) implies

$$\Omega(E) = \int_0^\infty d\phi W \mathcal{M}(\phi; E) \mathcal{D}(\phi) \approx W(E - \phi_E)^{\frac{3N}{2}} Z(\beta_E). \quad (34)$$

where $Z(\beta)$ is the configurational partition function, defined by

$$Z(\beta) := \int_0^\infty d\phi \mathcal{D}(\phi) \exp(-\beta\phi) = \frac{\Omega_0 \Gamma(\alpha + 1)}{W \Gamma(\frac{3N}{2})} \beta^{\frac{3N}{2} - \alpha - 1}. \quad (35)$$

Furthermore, replacing the approximations for $\mathcal{M}(\phi; E)$ and $\Omega(E)$ into (10), we see that

$$\rho(\phi; E) \approx \frac{W}{\Omega(E)} (E - \phi_E)^{\frac{3N}{2}} \exp(-\beta_E \phi) \approx \left[\frac{\exp(-\beta \phi)}{Z(\beta)} \right]_{\beta=\beta_E}, \quad (36)$$

that is, the ensemble function given E is that of a q -canonical distribution, as first shown by Naudts *et al* [16], such that it reduces to a canonical ensemble at inverse temperature β_E in the thermodynamic limit. In particular, the condition that for all energies E ,

$$\langle \phi \rangle_E = E \left(1 - \frac{3N}{2(\alpha + 1)} \right) \approx \langle \phi \rangle_{\beta=\beta_E} \quad (37)$$

with $\langle \phi \rangle_\beta$ the canonical expectation of the potential energy, allows us to fix the value of ϕ_E . We have

$$\langle \phi \rangle_\beta = -\frac{\partial}{\partial \beta} \ln Z(\beta) = \frac{\alpha R}{\beta} \quad (38)$$

where R is a constant defined by

$$R := 1 - \frac{3N}{2\alpha}, \quad (39)$$

therefore for $\alpha \gg 1$ the condition in (37) reduces to

$$E = \frac{2\alpha}{3N} (E - \phi_E) \quad (40)$$

with solution $\phi_E = RE$. We see that ϕ_E coincides with the most probable potential energy $\phi^*(E)$ in (15) for $N \gg 1$, and is such that

$$\beta_E = \frac{\alpha}{E} = \beta_\Omega(E), \quad (41)$$

thus there is no ambiguity in the value of inverse temperature. In summary, we have shown that (29) can be approximated in the thermodynamic limit by the superstatistical ensemble function

$$\rho(\phi; S) \approx \int_0^\infty d\beta P(\beta|S) \left[\frac{\exp(-\beta\phi)}{Z(\beta)} \right] \quad (42)$$

with a distribution of inverse temperatures given by

$$P(\beta|S) = \int_0^\infty dE P(E|S) \delta(\beta_\Omega(E) - \beta). \quad (43)$$

Replacing (35) in (42) and imposing normalization we finally obtain

$$P(\phi|S) \approx \frac{1}{\Gamma(\alpha + 1 - \frac{3N}{2})} \int_0^\infty d\beta P(\beta|S) \beta \cdot (\beta\phi)^{\alpha - \frac{3N}{2}} \exp(-\beta\phi). \quad (44)$$

4. Energy oscillations

To study the effect of energy oscillations in a finite-size system, for simplicity, we will consider that our system has a time-dependent total energy given by

$$E(t) = E_0 + A \sin(\omega t) \quad (45)$$

so that $E(t) \in [E_0 - A, E_0 + A]$. The probability of observing a value E is obtained from the time average

$$P(E|A, E_0, \omega) = \lim_{\tau \rightarrow \infty} \frac{1}{\tau} \int_0^\tau dt \delta(E - E(t)) = \lim_{\tau \rightarrow \infty} \frac{1}{\tau} \int_0^\tau dt \sum_{t_0} \frac{\delta(t - t_0)}{|E'(t_0)|} \quad (46)$$

where the times t_0 are such that

$$\sin(\omega t_0) = \frac{E - E_0}{A}. \quad (47)$$

By replacing

$$E'(t_0) = A\omega \cos(\omega t_0) = \omega \sqrt{A^2 - (E - E_0)^2} \quad (48)$$

in (46) we obtain the probability density

$$P(E|A, E_0) = \frac{1}{\pi} \frac{\Theta(A - |E - E_0|)}{\sqrt{A^2 - (E - E_0)^2}} = \frac{1}{\pi} \frac{\Theta(A - |E - E_0|)}{\sqrt{E - (E_0 - A)} \sqrt{(E_0 + A) - E}}, \quad (49)$$

which gives the energy fluctuations associated with the oscillation. Note that this distribution does not depend on the frequency of oscillation, only on the amplitude A and the reference energy E_0 .

The superstatistical distribution of inverse temperatures can be directly computed from (49) and (43), yielding

$$P(\beta|A, E_0) = \frac{1}{\pi\beta_0 \sqrt{\gamma^2(\beta/\beta_0)^4 - (\beta/\beta_0)^2(1 - \beta/\beta_0)^2}} \quad (50)$$

provided that

$$\frac{1}{1 + \gamma} < \frac{\beta}{\beta_0} < \frac{1}{1 - \gamma}, \quad (51)$$

where we have defined a reference inverse temperature $\beta_0 := \alpha/E_0$. The first and second moments of (50) are

$$\beta_S := \langle \beta \rangle_{A, E_0} = \frac{\beta_0}{\sqrt{1 - \gamma^2}}, \quad (52)$$

and

$$\langle \beta^2 \rangle_{A, E_0} = \frac{(\beta_S)^2}{\sqrt{1 - \gamma^2}}, \quad (53)$$

respectively, and from them we can compute the superstatistical relative variance of β as

$$u := \frac{\langle (\delta\beta)^2 \rangle_{A, E_0}}{\langle \beta \rangle_{A, E_0}^2} = \frac{1}{\sqrt{1 - \gamma^2}} - 1. \quad (54)$$

Direct calculation of the energy moments from (49) is cumbersome, and we will again make use of the conjugate variables theorem. For the case of the distribution $P(E|A, E_0)$ in (49) it reduces to

$$\left\langle \frac{\partial \omega}{\partial E} \right\rangle_{A, E_0} = - \left\langle \omega \left[\frac{E - E_0}{A^2 - (E - E_0)^2} \right] \right\rangle_{A, E_0}. \quad (55)$$

Under the choice $\omega(E) = g(E)[A^2 - (E - E_0)^2]$, where $g(E)$ is another arbitrary, differentiable function of E , we have

$$\left\langle \frac{\partial g}{\partial E} [A^2 - (E - E_0)^2] \right\rangle_{A, E_0} = \langle g(E)(E - E_0) \rangle_{A, E_0} \quad (56)$$

Using $g(E) = 1$ gives the mean energy as

$$\langle E \rangle_{A,E_0} = E_0, \quad (57)$$

while from $g(E) = E - E_0$ we obtain the energy variance

$$\langle (\delta E)^2 \rangle_{A,E_0} = \frac{A^2}{2}, \quad (58)$$

as expected from (45). A recurrence relation for the moments of E can be obtained from (56) under the choice $g(E) = E^m$, namely

$$m(\gamma^2 - 1)E_0^2 \langle E^{m-1} \rangle_{A,E_0} + (2m + 1)E_0 \langle E^m \rangle_{A,E_0} = (m + 1) \langle E^{m+1} \rangle_{A,E_0} \quad (59)$$

where we have introduced

$$\gamma := \frac{A}{E_0}. \quad (60)$$

In order to solve it, it is more convenient to compute the moment generating function for the variable $E - E_0$, defined by

$$M_{E-E_0}(t; A, E_0) := \langle \exp(t(E - E_0)) \rangle_{A,E_0}, \quad (61)$$

which can be obtained from (56) using $g(E) = \exp(t(E - E_0))$. This leads to

$$A^2 t \langle \exp(t[E - E_0]) \rangle_{A,E_0} - t \langle \exp(t[E - E_0])(E - E_0)^2 \rangle_{A,E_0} = \langle \exp(t[E - E_0])(E - E_0) \rangle_{A,E_0}, \quad (62)$$

which can be transformed into the second-order differential equation

$$A^2 t M_{E-E_0}(t; A, E_0) - t \frac{\partial^2}{\partial t^2} M_{E-E_0}(t; A, E_0) = \frac{\partial}{\partial t} M_{E-E_0}(t; A, E_0) \quad (63)$$

with solution

$$M_{E-E_0}(t; A, E_0) = I_0(At) \quad (64)$$

where I_0 is the modified Bessel function of the first kind. The moment generating function for E follows directly from (64), as

$$M_E(t; A, E_0) := \langle \exp(tE) \rangle_{A,E_0} = \exp(tE_0) M_{E-E_0}(t; A, E_0) = \exp(tE_0) I_0(At), \quad (65)$$

and from it we can extract the moments

$$\langle E^m \rangle_{A,E_0} = {}_2F_1\left(\frac{1-m}{2}, -\frac{m}{2}, 1; \gamma^2\right) E_0^m, \quad (66)$$

in which ${}_2F_1$ corresponds to the Gauss hypergeometric function, for $m \geq 0$. We will now compute the inverse temperature covariance \mathcal{U} , introduced in Ref. [8] and defined by

$$\mathcal{U} := \langle (\delta\beta_\Omega)^2 \rangle_S + \langle \beta_\Omega' \rangle_S, \quad (67)$$

and which is relevant to determine the superstatistical regime. In superstatistics, \mathcal{U} is equal to the variance of the superstatistical parameter β , so $\mathcal{U} \geq 0$ and from (54) we expect that

$$\mathcal{U} \approx \langle (\delta\beta)^2 \rangle_{A,E_0} = (\beta_S)^2 \left[\frac{1}{\sqrt{1-\gamma^2}} - 1 \right]. \quad (68)$$

For the computation of \mathcal{U} we need the expected values of $\langle E^{-1} \rangle_{A,E_0}$ and $\langle E^{-2} \rangle_{A,E_0}$, and because the moments in (66) are solutions of the recurrence relation in (59), they are also valid for $m < 0$. The expectation of β_Ω can be computed using $m = -1$ in (66), giving

$$\langle \beta_\Omega \rangle_{A,E_0} = \left\langle \frac{\alpha}{E} \right\rangle_{A,E_0} = \frac{\beta_0}{\sqrt{1-\gamma^2}} = \beta_S. \quad (69)$$

We see then that β_S increases, i.e. the steady state temperature decreases, with γ . From this result for β_S , and using (7), we can write the generalized equation of state

$$\langle E \rangle_{A,E_0} = \frac{C_E}{\sqrt{1-\gamma^2}} T_S, \quad (70)$$

where we have a generalized heat capacity

$$C_S := \frac{C_E}{\sqrt{1-\gamma^2}} \geq C_E. \quad (71)$$

Using $m = -2$ in (66), we readily have

$$\langle E^{-2} \rangle_{A,E_0} = \frac{1}{E_0^2} \frac{1}{(\sqrt{1-\gamma^2})^3}, \quad (72)$$

so we can write

$$\langle (\delta\beta_\Omega)^2 \rangle_{A,E_0} = \alpha^2 \langle E^{-2} \rangle_{A,E_0} - \beta_S^2, \quad (73a)$$

$$\langle \beta_\Omega' \rangle_{A,E_0} = -\alpha \langle E^{-2} \rangle_{A,E_0}. \quad (73b)$$

After some algebra, we obtain

$$\mathcal{U} = u (\beta_S)^2 \quad (74)$$

with

$$u = \frac{\alpha - 1}{\alpha \sqrt{1-\gamma^2}} - 1. \quad (75)$$

As expected, the reduced inverse temperature covariance increases with γ , as the system is driven further away from equilibrium. There is a critical value of γ , namely

$$\gamma_c := \frac{\sqrt{2\alpha - 1}}{\alpha} \quad (76)$$

such that $\gamma > \gamma_c$ leads to $u > 0$, making the ensemble supercanonical. Note also that

$$\lim_{\alpha \rightarrow \infty} u = \frac{1}{\sqrt{1-\gamma^2}} - 1 \geq 0, \quad (77)$$

therefore in that limit we have agreement with (54). The threshold γ_c goes to zero as $\alpha \rightarrow \infty$, consistent with the idea that, in the thermodynamic limit, the ensemble must be compatible with superstatistics, and therefore must have $u > 0$ for all γ . On the other hand, for vanishing oscillation amplitude we have

$$\lim_{\gamma \rightarrow 0} u = -\frac{1}{\alpha}, \quad (78)$$

recovering the microcanonical result. Alternatively, we can obtain u and β_S from

$$\beta_S = \langle b_\Omega \rangle_{A,E_0} \quad (79)$$

and

$$u = \frac{\langle (\delta b_\Omega)^2 \rangle_{A,E_0} + \langle b_\Omega' \rangle_{A,E_0}}{\langle b_\Omega \rangle_{A,E_0}} \quad (80)$$

where

$$b_\Omega(\phi) := \frac{\partial}{\partial \phi} \ln \mathcal{D}(\phi) = \frac{2\alpha - 3N}{2\phi}. \quad (81)$$

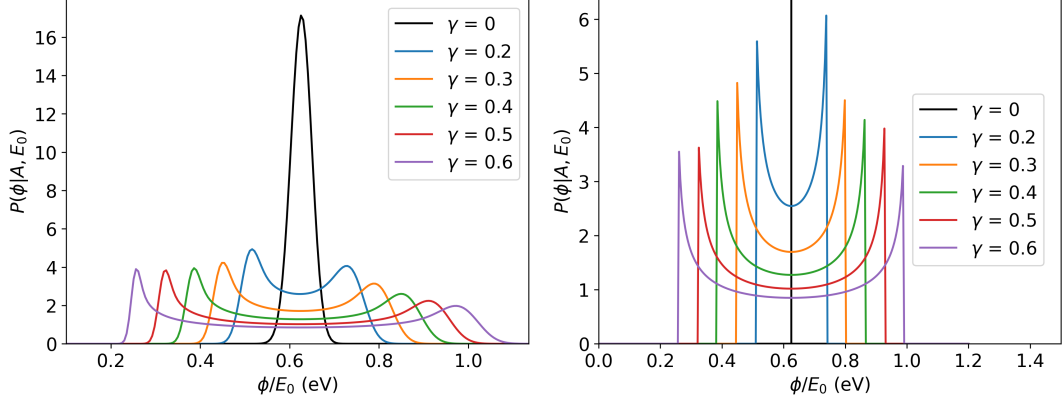


Figure 1: Left, exact probability density $P(\phi|A, E_0)$ in (83) evaluated numerically for $N = 108$. Right, asymptotic probability density $P(\phi|A, E_0)$ as given in (95).

The exact distribution of potential energies for any value of A and any system size N is given by marginalization of the energy variable E , that is, by the integral

$$P(\phi|A, E_0) = \int_0^\infty dE P(E|A, E_0) P(\phi|E). \quad (82)$$

Replacing (49) and (13) we can write

$$P(\phi|A, E_0) = \frac{\left(\frac{\phi}{E_0}\right)^{\alpha - \frac{3N}{2}} \mathcal{K}\left(\frac{\phi}{E_0}; \gamma, \alpha, N\right)}{E_0 \pi B\left(\frac{3N}{2}, \alpha + 1 - \frac{3N}{2}\right)} \quad (83)$$

where we have defined the special function

$$\mathcal{K}(z; \gamma, \alpha, N) := \int_{\max(z, 1-\gamma)}^{1+\gamma} \frac{dx x^{-\alpha} (x-z)^{\frac{3N}{2}-1}}{\sqrt{x-(1-\gamma)} \sqrt{(1+\gamma)-x}}. \quad (84)$$

The distribution in (83) does not seem to have a closed form but can be evaluated numerically, as shown in Fig. 1. We can see curves for several values of γ ranging from 0 to 0.6 on both the left and right panels. On the left panel, corresponding to the exact probability density in (83), we can observe that the distribution has a Gaussian shape when no driving ($\gamma = 0$) is considered. Two clear peaks and a valley develop when γ is increased, and accordingly the variance of ϕ also increases. On the right side panel, showing the asymptotic probability density, two sharp peaks appear for non-zero values of γ , and again a deep valley forms between those peaks. Thus the behavior is an extreme form of the features observed for the exact density.

Despite the fact that (83) seems intractable, the moments of $P(\phi|A, E_0)$ can be computed in closed form using (19) together with the marginalization rule

$$\langle \phi^m \rangle_{A, E_0} = \int_0^\infty dE P(E|A, E_0) \langle \phi^m \rangle_E. \quad (85)$$

We obtain

$$\langle \phi^m \rangle_{A, E_0} = \frac{\Gamma(\alpha + 1) \Gamma(\alpha + m + 1 - \frac{3N}{2})}{\Gamma(\alpha + m + 1) \Gamma(\alpha + 1 - \frac{3N}{2})} \langle E^m \rangle_{A, E_0}, \quad (86)$$

which upon replacing (66) becomes

$$\langle \phi^m \rangle_{A, E_0} = {}_2F_1\left(\frac{1-m}{2}, -\frac{m}{2}, 1; \gamma^2\right) \cdot E_0^m \frac{\Gamma(\alpha + 1) \Gamma(\alpha + m + 1 - \frac{3N}{2})}{\Gamma(\alpha + m + 1) \Gamma(\alpha + 1 - \frac{3N}{2})}, \quad (87)$$

that is,

$$\langle \phi^m \rangle_{A,E_0} = {}_2F_1\left(\frac{1-m}{2}, -\frac{m}{2}, 1; \gamma^2\right) \cdot \langle \phi^m \rangle_{E_0}. \quad (88)$$

Clearly we recover the microcanonical result for $\gamma = 0$ because ${}_2F_1(a, b, c; 0) = 1$ for all a, b, c . Similarly, because ${}_2F_1(0, b, c; z) = 1$ for all b, c, z it readily follows that

$$\langle \phi \rangle_{A,E_0} = \langle \phi \rangle_{E_0} = E_0 \left[1 - \frac{3N}{2(\alpha + 1)} \right]. \quad (89)$$

Here we can see that the mean potential energy is not affected by the amplitude of oscillation of the total energy. The relative variance of ϕ given A and E_0 is

$$\frac{\langle (\delta\phi)^2 \rangle_{A,E_0}}{\langle \phi \rangle_{A,E_0}^2} = \frac{1}{2} \left(\frac{\alpha + 1}{\alpha + 2} \right) \left(\frac{\alpha + 2 - \frac{3N}{2}}{\alpha + 1 - \frac{3N}{2}} \right) (\gamma^2 + 2) - 1, \quad (90)$$

and can see that (90) agrees with (21) when $\gamma \rightarrow 0$. Moreover, it follows that the variance cannot decrease with respect to the one in (21), that is,

$$\langle (\delta\phi)^2 \rangle_{A,E_0} \geq \langle (\delta\phi)^2 \rangle_{E_0}. \quad (91)$$

The result in (88), as well as those in (89) and (90) are exact for all sizes $N \geq 1$. The limit $N \rightarrow \infty$ of (90) yields

$$\lim_{N \rightarrow \infty} \frac{\langle (\delta\phi)^2 \rangle_{A,E_0}}{\langle \phi \rangle_{A,E_0}^2} = \frac{\gamma^2}{2}. \quad (92)$$

Similarly, for $N \gg 1$, we can use Stirling's approximation to obtain

$$\langle \phi^m \rangle_{A,E_0} \approx (RE_0)^m {}_2F_1\left(\frac{1-m}{2}, -\frac{m}{2}, 1; \gamma^2\right), \quad (93)$$

with R as defined in (39), and this implies that the distribution of the dimensionless variable

$$z := \frac{\phi}{RE_0} \quad (94)$$

only depends on γ . Comparison of the approximate moments in (93) with the exact moments (66) of the distribution in (49) tells us that ϕ/R follows the same distribution as E , therefore we can write

$$P(\phi|A, E_0) \approx \frac{1}{\pi RE_0} \frac{\Theta(\gamma - |z - 1|)}{\sqrt{z - (1 - \gamma)} \sqrt{1 + \gamma - z}}, \quad (95)$$

and, in this approximation, z is constrained to the interval

$$1 - \gamma \leq z \leq 1 + \gamma. \quad (96)$$

5. Molecular dynamics simulation

Computational simulations of a Lennard-Jones (LJ) crystal were performed to evaluate its potential energy distribution. Several different values of A ranging from 0 to 2 were considered in order to establish a clear connection between the simulations and the distributions for inverse temperature and potential energy. The simulations were performed using a homemade software written in the Rust computational language [17] for efficiency. For each value of A , several classical dynamics simulations were performed. The simulation consists of Ar atoms with a lattice constant $a = 5.256 \text{ \AA}$ in an FCC structure with 108 atoms. The interatomic potential used in the molecular dynamics simulations is the well-known Lennard-Jones pair potential, where

$$\Phi(\mathbf{r}_1, \dots, \mathbf{r}_N) = \sum_{i=1}^N \sum_{j<i}^N V(|\mathbf{r}_i - \mathbf{r}_j|) \quad (97)$$

with

$$V(r) = 4\epsilon \left[\left(\frac{\sigma}{r} \right)^{12} - \left(\frac{\sigma}{r} \right)^6 \right]. \quad (98)$$

Here ϵ is the depth of the potential well, σ is the finite distance at which the inter-particle potential is zero, and r is the distance between the particles. In our case, the parameters were used, namely $\epsilon/k_B = 120$ K, and $\sigma = 3.4$ Å [18, 19]. The potential energy of the ideal crystal, denoted by ϕ_0 , must be subtracted from the simulation data for consistency with the assumptions of our model, where zero temperature must correspond to zero total energy. The values of the properties defining the LJ system are summarized in Table 1.

Table 2 shows the parameters used in some of the molecular dynamics runs and the values of the corresponding thermodynamical properties.

| N | a (Å) | σ (Å) | ϵ (K $\cdot k_B$) | ϕ_0 (eV) | α/N | γ_c |
|-----|---------|--------------|-----------------------------|---------------|------------|------------|
| 108 | 5.256 | 3.4 | 120 | -17.581 | 4.1652 | 0.0666413 |

Table 1: Properties of the LJ system used in molecular dynamics simulations.

| Run | A (eV) | T_0 (K) | E_0 (eV) | γ | T_S (K) | T_S^\dagger (K) |
|-----|----------|-----------|------------|----------|-----------|-------------------|
| 509 | 0.5 | 50 | 2.1643 | 0.2303 | 54.33152 | 56.96488 |
| 505 | 0.7 | 50 | 2.1411 | 0.3259 | 52.21707 | 54.79973 |
| 501 | 1.1 | 50 | 2.1770 | 0.5037 | 48.51658 | 51.03723 |
| 468 | 0.1 | 100 | 3.9725 | 0.0271 | 102.4402 | 103.5647 |
| 447 | 0.3 | 100 | 3.7981 | 0.0792 | 97.67073 | 100.8323 |
| 450 | 0.5 | 100 | 3.9976 | 0.1249 | 102.3180 | 105.4649 |
| 454 | 0.7 | 100 | 3.9634 | 0.1762 | 100.6439 | 103.7880 |
| 465 | 1.1 | 100 | 4.0459 | 0.2710 | 100.4638 | 103.6523 |
| 514 | 1.7 | 100 | 4.4135 | 0.3840 | 105.1264 | 108.3611 |
| 515 | 2.0 | 100 | 4.4395 | 0.4491 | 102.3233 | 105.5759 |
| 511 | 0.5 | 150 | 6.6426 | 0.0755 | 170.8695 | 173.2787 |
| 507 | 0.7 | 150 | 6.8160 | 0.1027 | 174.9016 | 177.2377 |
| 503 | 1.1 | 150 | 5.8826 | 0.1865 | 149.0887 | 151.8897 |
| 512 | 0.5 | 200 | 9.2725 | 0.0546 | 238.8443 | 240.1096 |
| 508 | 0.7 | 200 | 7.8657 | 0.0891 | 202.1019 | 203.9980 |
| 504 | 1.1 | 200 | 8.9802 | 0.1224 | 229.9184 | 231.3308 |

Table 2: Parameters used in several molecular dynamics simulation runs, together with measured properties. The value T_S^\dagger is computed from the expression in (79).

Once the potential energy data is extracted from the simulations, we analyze its statistical distribution in order to compare them with the theoretical results of the superstatistical framework. Fig. 2 shows the mean potential energy as a function of total energy for several values of γ . We confirm the linear relationship predicted by (20) and the fact that the mean potential energy is independent of γ . From the slope of the line we have determined $\alpha = 4.1652$ per atom.

Fig. 3 compares the predictions of superstatistics with the molecular dynamics simulation. The left panel shows the agreement between the expected distribution of inverse temperatures and the empirical distribution from molecular dynamics. In the right panel, the superstatistical probability density for ϕ is compared with the empirical distribution from run 515 of Table 2, and we see a precise agreement even for $N = 108$ atoms. Similarly, Fig. 4 shows the relationship between u and γ as predicted in (75), together with the superstatistical limit in (54) and the values computed from molecular dynamics simulations.

Finally, Figs. 5 to 7 depict the potential energy distributions observed in some of the molecular dynamics runs with parameters in Table 2, together with the exact and superstatistical predictions. First, the left panel of Fig. 5 shows the case of $\gamma = 0.0271$ and $E_0 = 3.9725$ eV, corresponding to run 468. A Gaussian shape is observed here for

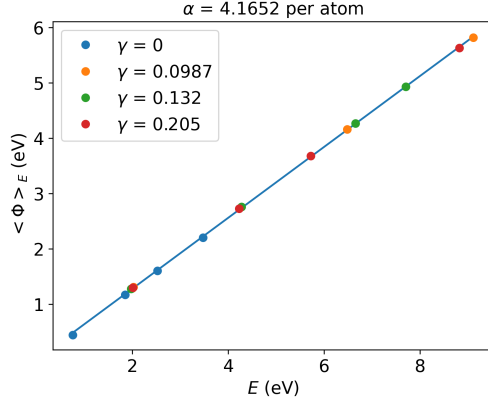


Figure 2: Mean potential energy as a function of total energy for several values of γ , that is, corresponding to (89).

both the simulation and the exact curve. On the right panel, we see the results for $\gamma = 0.0792$ and $E_0 = 3.7981$ eV, corresponding to run 447. As γ increases, the exact curve clearly defines two main peaks, which are moving to the boundaries of the asymptotic solution. For the case of simulation data, a more spread distribution is observed, and a clear peak can be easily defined, which suggests a transition of the distribution to a more complex one. Fig. 6 presents two particular cases, in the left panel with $\gamma = 0.1248$ and $E_0 = 3.9974$ eV corresponding to run 450, while in the right panel we see the results from run 454, with $\gamma = 0.1762$ and $E_0 = 3.9632$ eV.

The left panel of Fig. 7 shows the distribution of potential energies for $\gamma = 0.2710$ and $E_0 = 4.0459$ eV, corresponding to run 465, while the right panel shows the results from run 515, having $\gamma = 0.4491$ and $E_0 = 4.4395$ eV.

Here we can see that for high enough values of γ the agreement between the simulation data and the predictions improves. Still we can notice significant deviations from the asymptotic approximation, particularly at the high-energy tails, where the exact and superstatistical distribution provide a more accurate description of the simulation data. This highlights the limitations of the asymptotic approximation in capturing the true behavior of potential energy distributions in finite-size systems. The exact numerical evaluation aligns closely with the simulation results, particularly at low energies, but not as expected at high energy, where an elongated tail is observed for the simulation data. Despite these, our results present a reasonable agreement, validating its effectiveness in modeling these systems.

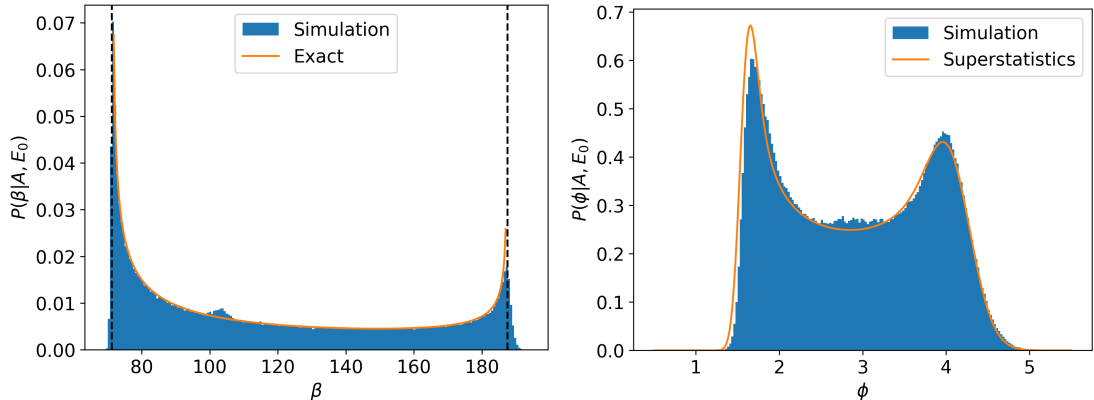


Figure 3: Left, empirical distribution of inverse temperature β_Ω versus (50). Right, superstatistical distribution of potential energies given by (44) versus the empirical distribution from molecular dynamics simulation.

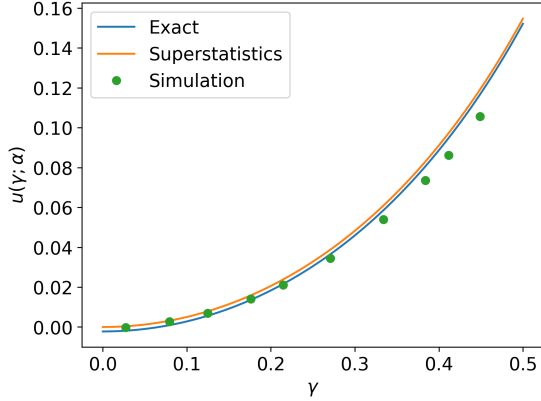


Figure 4: Reduced inverse temperature correlation u as a function of γ for $N = 108$ atoms and $\alpha/N = 4.1652$. The blue curve is the exact prediction in (75), while the orange curve is the asymptotic approximation in (77). The green circles represent values computed from molecular dynamics simulations using (80).

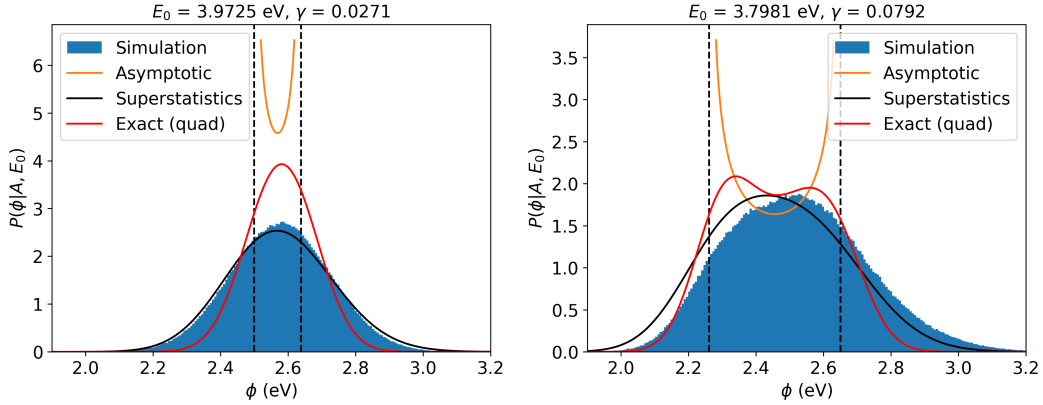


Figure 5: Left, distribution of potential energies for $\gamma = 0.0271$ and $E_0 = 3.9725$ eV, corresponding to run 468 in Table 2. Right, $\gamma = 0.0792$ and $E_0 = 3.7981$ eV, corresponding to run 447. The orange curve is the asymptotic approximation in (95), while the red curve is the exact distribution in (83) evaluated numerically and the black curve is the superstatistical distribution in (44).

6. Concluding remarks

In this study, we have successfully demonstrated the applicability of superstatistics to the thermodynamic behavior of finite, driven classical systems. By employing classical molecular dynamics simulations, we validated the theoretical framework of steady-state statistical mechanics and superstatistics for the description of the potential energy distributions observed under external energy fluctuations.

The agreement between the molecular dynamics simulations and the theoretical predictions clearly illustrates the robustness of the superstatistical approach. The analysis in terms of the inverse temperature covariance \mathcal{U} and its dependence on the relative oscillation amplitude γ provides information about the superstatistical regime. We confirm that the reduced inverse temperature covariance u increases with γ and for values exceeding a critical threshold γ_c , the system transitions to a regime where the superstatistical description becomes more pertinent. This finding is important in order to understand the conditions under which superstatistics is applicable even in the case of driven systems. In short, our results provide a fundamental connection between superstatistics and steady-state, finite-size thermodynamics, which opens the way for new applications of superstatistics in condensed matter physics.

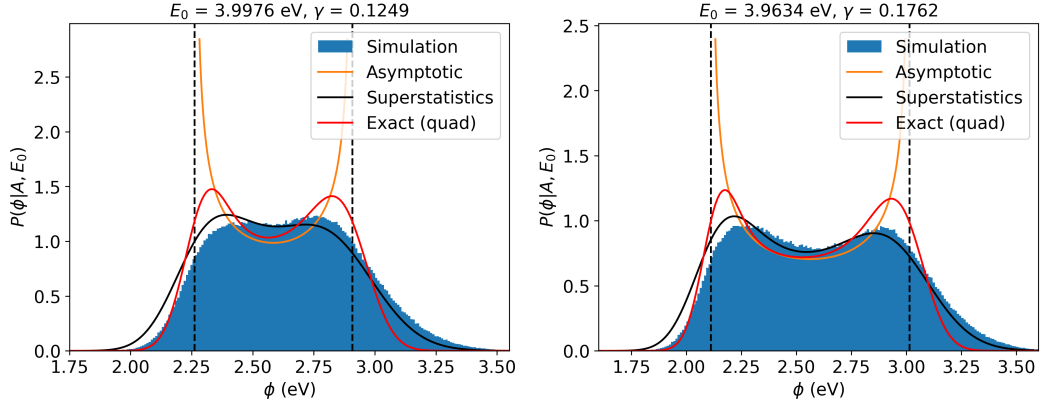


Figure 6: Left, distribution of potential energies for $\gamma = 0.1249$ and $E_0 = 3.9976$ eV, corresponding to run 450 in Table 2. Right, $\gamma = 0.1762$ and $E_0 = 3.9634$ eV, corresponding to run 454. The orange curve is the asymptotic approximation in (95), while the red curve is the exact distribution in (83) evaluated numerically and the black curve is the superstatistical distribution in (44).

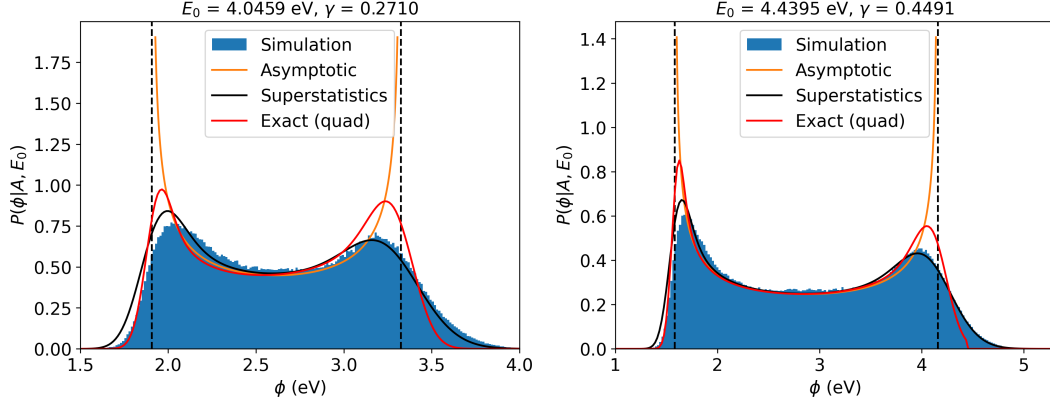


Figure 7: Left, distribution of potential energies for $\gamma = 0.2710$ and $E_0 = 4.0459$ eV, corresponding to run 465 in Table 2. Right, $\gamma = 0.4491$ and $E_0 = 4.4395$ eV, corresponding to run 515. The orange curve is the asymptotic approximation in (95), while the red curve is the exact distribution in (83) evaluated numerically and the black curve is the superstatistical distribution in (44).

Acknowledgments

Funding from ANID FONDECYT 1220651 is gratefully acknowledged. This computational work was supported by the NLHPC (ECM-02) and FENIX (UNAB) supercomputing infrastructures.

Appendix A. Configurational density of states

In the following, we will deduce the form in (12) for the configurational density of states of a system with constant microcanonical heat capacity. First, consider the canonical partition function $Z(\beta)$ written in terms of the density of states $\Omega(E)$, that is,

$$Z(\beta) = \int_0^\infty dE \Omega(E) \exp(-\beta E). \quad (\text{A.1})$$

As is well-known, for a Hamiltonian as in (1) the partition function is the product of a kinetic part, denoted by $Z_K(\beta)$ and a configurational part, $Z_\Phi(\beta)$, thus

$$Z(\beta) = Z_K(\beta) Z_\Phi(\beta) \quad (\text{A.2})$$

with

$$Z_{\Phi}(\beta) = \int_0^{\infty} d\phi \mathcal{D}(\phi) \exp(-\beta\phi) \quad (\text{A.3})$$

and where the kinetic part is given by

$$Z_K(\beta) = \int_0^{\infty} dK \Omega_K(K) \exp(-\beta K) = \int_0^{\infty} dK (WK^{\frac{3N}{2}-1}) \exp(-\beta K) = W\Gamma(3N/2)\beta^{-\frac{3N}{2}}, \quad (\text{A.4})$$

after replacing (4). By replacing (9) into (A.1) we readily have

$$Z(\beta) = \Omega_0\Gamma(\alpha + 1)\beta^{-(\alpha+1)}, \quad (\text{A.5})$$

and therefore the configurational part of the partition function is given by

$$Z_{\Phi}(\beta) = \frac{Z(\beta)}{Z_K(\beta)} = \frac{\Omega_0\Gamma(\alpha + 1)}{W\Gamma(3N/2)}\beta^{-\alpha-1+\frac{3N}{2}}. \quad (\text{A.6})$$

Applying the inverse Laplace transform to (A.3) and replacing (A.6) we finally obtain

$$\mathcal{D}(\phi) = D_0 \phi^{\alpha-\frac{3N}{2}} \quad (\text{A.7})$$

with

$$D_0 = \frac{\Omega_0\Gamma(\alpha + 1)}{W\Gamma(3N/2)\Gamma(\alpha - 3N/2 + 1)}. \quad (\text{A.8})$$

References

- [1] P. D. Dixit. *J. Chem. Phys.*, 138:184111, 2013.
- [2] P. D. Dixit. *Phys. Chem. Chem. Phys.*, 17:13000–13005, 2015.
- [3] L. Herron and P. D. Dixit. *J. Stat. Mech.: Theor. Exp.*, 2021:33207, 2021.
- [4] C. Beck and E.G.D. Cohen. *Phys. A*, 322:267–275, 2003.
- [5] C. Beck. *Cont. Mech. Thermodyn.*, 16:293–304, 2004.
- [6] F. Ritort. *Adv. Chem. Phys.*, 137:31–123, 2007.
- [7] F. Sattin. *Eur. Phys. J. B*, 49:219–224, 2006.
- [8] S. Davis. *Phys. A*, 589:126665, 2022.
- [9] C. Farías and S. Davis. *Eur. Phys. J. B*, 96:39, 2023.
- [10] E. S. Severin, B. C. Freasier, N. D. Hamer, D. L. Jolly, and S. Nordholm. *Chem. Phys. Lett.*, 57:117–120, 1978.
- [11] E. M. Pearson, T. Halicioğlu, and W. A. Tiller. *Phys. Rev. A*, 32:3030–3039, 1985.
- [12] J. R. Ray. *Phys. Rev. A*, 44:4061–4064, 1991.
- [13] S. Davis and G. Gutiérrez. *Phys. Rev. E*, 86:051136, 2012.
- [14] S. Davis and G. Gutiérrez. *AIP Conf. Proc.*, 1757:20002, 2016.
- [15] J. L. Lebowitz, J. K. Percus, and L. Verlet. *Phys. Rev.*, 153:250–254, 1967.
- [16] J. Naudts and M. Baeten. *Entropy*, 11:285–294, 2009.
- [17] N. D. Matsakis and F. S. Klock. *The Rust Programming Language*, 2014. Available at <https://www.rust-lang.org/>.
- [18] M. P. Allen and D. J. Tildesley. *Computer Simulation of Liquids*. Oxford University Press, 1989.
- [19] D.C. Rapaport. *The Art of Molecular Dynamics Simulation*. Cambridge University Press, 2004.